

3
4 **Computational analysis for good thermal**
5 **exchange and low pressure drop in**
6 **regenerative air preheaters**
7

8
9
10
11 **ABSTRACT**
12

A computational analysis in a rotary regenerative air preheater is performed. The total heat transfer, the pressure drop and the outlet temperatures of streams in the equipment are calculated from different matrix porosity values and the pre-established mass flow rates. Three typical regenerative air preheaters sizes are simulated. The heat transfer coefficient in the exchanger and the friction factor are obtained from correlations. The total heat transfer is obtained using the Effectiveness-NTU method specific to regenerative air preheaters. The results allow to identify, for each simulated case, the porosity values that provide good thermal exchange and low pressure drop in the equipment. Besides that, the behavior of the outlet temperatures of each gas stream as function of the porosity is also investigated.

13
14 *Keywords: regenerative air preheater, heat transfer, pressure drop, simulation.*
15

16 **1. INTRODUCTION**
17

18 Regenerative air preheaters are used in many heat recovery systems. Its range of applications
19 encompasses refrigeration systems, ventilation plants, thermal comfort, power plant boilers,
20 recovery of waste thermal energy and a number of situations where the availability of the
21 energy does not chronologically coincide with demand [1].
22

23 Over the years, researchers have focused efforts on improving this heat exchanger due to
24 some of its advantages such as compactness, efficiency, economy and high flexibility. The
25 studies found in the literature incorporate various aspects of the equipment. The pioneer
26 works about the regenerative air preheater were essentially experimental with investigations
27 that mainly included the effectiveness, the thermal exchange and the pressure drop [2–5].
28 Later studies to the most recent ones include aspects of the equipment such as
29 mathematical modeling and numerical analysis [6-9], mass transfer [10-13], leakage control
30 [14-16], thermodynamic analysis [17-19], rotational speed of the matrix [20-22] and geometry
31 of matrix ducts [23-26].
32

33 Analysis from the matrix porosity of the regenerative air preheater are found in a small
34 number of works [27-31]. The present study analyzes three typical regenerative air
35 preheaters. The aim is select the porosity values that provide good thermal exchange and
36 low pressure drop in the equipment. Additionally, the behavior of the outlet temperatures of
37 each gas stream as function of the porosity is also investigated.
38

39 **2. PROBLEM DESCRIPTION AND METHODOLOGY**

40

41 **2.1 Characterization of the Regenerative Air Preheater**

42

43 The schematic of the regenerative air preheater is shown in Fig. 1. Two gas streams are
44 introduced counterflow-wise through the parallel ducts of the air preheater. Cold gas is
45 injected inside one duct and hot gas inside the other. The porous matrix, that stores energy,
46 continuously rotates through these parallel ducts. The matrix receives heat from the hot gas
47 on one side and transfers this energy to the cold gas on the other side. The matrix channels
48 were assumed smooth. The fluid velocity was considered constant inside each channel.

49

50

51

52

53

54

55

56

57

58

59

60

61

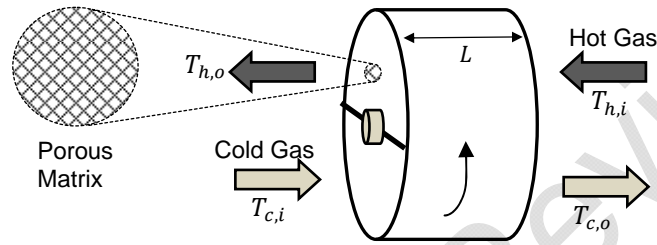


Fig. 1. Schematic of the regenerative air preheater.

62

63

64

65

66

67

68

69

70

71

72

73

74

75

76

77

78

79

80

81

82

83

84

Some geometric parameters can be expressed based on Fig. 1. The total frontal cross-sectional area A_T is determined by the sum of the free flow cross-sectional area A and the matrix cross-sectional area A_m of the air preheater

$$A_T = A + A_m \quad (1)$$

The matrix porosity σ is defined by the ratio between A and A_T

$$\sigma = \frac{A}{A_T} \quad (2)$$

The hydraulic radius r_h is defined by the ratio between A and the perimeter P of the plates that compose the matrix. The matrix perimeter can be written as function of the matrix cross-sectional area A_m

$$r_h = \frac{D_h}{4} = \frac{A}{P} \quad (3)$$

$$P = \frac{A_m}{(e/2)} \quad (4)$$

where D_h and e are the matrix duct hydraulic diameter and the matrix duct wall thickness, respectively.

The porosity and the hydraulic radius are dependent on each other and influence the thermal exchange in the regenerative air preheater. The hydraulic radius can be written as function

85 of the porosity and the matrix duct wall thickness from the definitions above and algebraic
86 manipulations
87

$$88 \quad r_h = \frac{\sigma}{1-\sigma} \left(\frac{e}{2} \right) \quad (5)$$

89
90 The hydraulic radius is an important parameter and its use is justified in the correlations for
91 friction factor and Nusselt number. Since the geometric characteristics of the regenerator are
92 known, the heat transfer in the equipment can be calculated using the Effectiveness-NTU
93 method for rotary regenerators.

94

95 **2.2 Effectiveness-NTU Method for Regenerative Air Preheaters**

96

97 The Effectiveness-NTU method for regenerative air preheaters [21] consists of calculating
98 the effectiveness ε_0 of a conventional counterflow heat exchanger and correcting this
99 effectiveness by a correction factor φ_r that takes into account the rotational speed and the
100 matrix heat capacity rate of the exchanger. Thus, the effectiveness of the regenerator ε_r is
101 given by

102

$$103 \quad \varepsilon_r = \varepsilon_0 \varphi_r \quad (6)$$

104

105 The effectiveness ε_0 of a conventional counterflow heat exchanger is defined by

106

$$107 \quad \varepsilon_0 = \frac{1 - \exp[-NTU(1 - C^*)]}{1 - C^* \exp[-NTU(1 - C^*)]} \quad (7)$$

108

109 where C^* is the ratio between the fluids heat capacity rates and NTU is the number of heat
110 transfer units defined as follows

111

$$112 \quad C^* = \frac{C_{min}}{C_{max}} \quad (8)$$

113

$$114 \quad NTU = \frac{I}{C_{min}} \left[\frac{I}{(I/hA_{tr})_c + (I/hA_{tr})_h} \right] \quad (9)$$

115

116 where h is the convective heat transfer coefficient and A_{tr} is the matrix thermal exchange
117 area on the side of the hot or cold stream. The parameters C_{min} and C_{max} correspond to the
118 minimum and maximum values of the fluids heat capacity rates.

119

120 The correction factor φ_r in Eq. (6) is given by

121

$$122 \quad \varphi_r = \frac{I}{9C_r^{*1.93}} \quad (10)$$

123

124 $C_r^* = \frac{C_r}{C_{min}} \quad (11)$

125

126 $C_r = \frac{n}{60} m_m c_m \quad (12)$

127

128 where C_r is the matrix heat capacity rate, n is the matrix rotational speed, m_m is the matrix
129 mass and c_m is the specific heat of matrix.

130

131 Finally, the total heat transfer Q in the air preheater is obtained in the same way as the
132 Effectiveness-NTU method for conventional heat exchangers

133

134 $Q = \varepsilon_r Q_{max} \quad (13)$

135

136 $Q_{max} = C_{min} (T_{h,i} - T_{c,i}) \quad (14)$

137

138 where Q_{max} is the maximum possible heat transfer and the term between parenthesis
139 corresponds to the difference between the inlet temperature of the hot stream and the inlet
140 temperature of the cold stream.

141

142 **2.3 Hydrodynamic and Thermal Analysis**

143

144 The hydrodynamic and thermal analysis are performed for each gas stream. The pressure
145 drop in the matrix ducts and the convective heat transfer coefficient are obtained from
146 correlations for Darcy friction factor f and Nusselt number Nu . Correlations for smooth
147 ducts with circular cross-sectional area were used based on the hydraulic diameter of matrix
148 ducts for laminar flow regime. The correlations take into account hydrodynamically fully
149 developed flow with thermal entrance length and constant wall temperature boundary
150 condition.

151

152 $f = \frac{64}{Re_{D_h}} \quad (15)$

153

154 $Nu = 3.66 + \frac{0.0668 \left(\frac{D_h}{L} \right) Re_{D_h} Pr}{1 + 0.04 \left[\left(\frac{D_h}{L} \right) Re_{D_h} Pr \right]^{\frac{2}{3}}} \quad (16)$

155

156 where L is the length of matrix, Re_{D_h} is the Reynolds number and Pr is the Prandtl number.

157

158 The distributed pressure drop ΔP is given by equation of Darcy-Weisbach and the
159 convective heat transfer coefficient h is expressed in terms of Nusselt number

160

161 $\Delta P = f \rho \frac{L}{D_h} \frac{V^2}{2} \quad (17)$

162

163 $h = \frac{Nu k}{D_h} \quad (18)$

164

165 where V , ρ and k are the fluid velocity, the fluid density and the fluid thermal conductivity,
166 respectively.

167

168 **2.4 Fluid and Matrix Properties**

169

170 The fluid properties were obtained at the average temperature of each gas stream. The fluid
171 density for gases with moderate values of pressure and temperature is well represented by
172 the equation of state of an ideal gas

173

174 $\rho = \frac{p}{RT} \quad (19)$

175

176 where p is the pressure of fluid, T is the average temperature of gas stream and R is the
177 ideal gas constant. The values of air atmospheric pressure $p = 10^5 Pa$ and ideal gas
178 constant for air $R = 287 Nm/kgK$ were assumed.

179

180 The dynamic viscosity μ and the thermal conductivity k of fluids can be approximated by
181 the Sutherland equations [32] as follows

182

183 $\frac{\mu}{\mu_0} \approx \left(\frac{T}{T_0} \right)^{3/2} \frac{T_0 + S}{T + S} \quad (20)$

184

185 $\frac{k}{k_0} \approx \left(\frac{T}{T_0} \right)^{3/2} \frac{T_0 + S}{T + S} \quad (21)$

186

187 where S is the Sutherland constant temperature, which is characteristic of each gas.
188 Considering air, $S = 111 K$ for dynamic viscosity and $S = 194 K$ for thermal conductivity. The
189 parameters T_0 , μ_0 and k_0 are reference constants, whose values are $T_0 = 273 K$,
190 $\mu_0 = 1.716 \cdot 10^{-5} Pa \cdot s$ and $k_0 = 0.0241 W/mK$ for air.

191

192 The specific heat of gas under constant pressure c_p is obtained by a polynomial equation [33]
193 with application for several gases in the temperature range between 300 and 1,000 K

194

195 $\frac{c_p}{R} = \alpha_0 + \beta_0 T + \gamma_0 T^2 + \delta_0 T^3 + \lambda_0 T^4 \quad (22)$

196

197 where $\alpha_0 = 3.653$, $\beta_0 = -1.337 \cdot 10^{-3}$, $\gamma_0 = 3.294 \cdot 10^{-6}$, $\delta_0 = -1.913 \cdot 10^{-9}$ and $\lambda_0 = 0.2763 \cdot 10^{-12}$
198 are the constants for the air.

199

200 The Prandtl number Pr is obtained from the ratio between some fluid properties, as follow
201

$$202 \quad Pr = \frac{\mu c_p}{k} \quad (23)$$

203

204 The matrix properties of the regenerative air preheater were assumed constant. The AISI
205 1010 low alloy carbon steel and the 2024-T6 aluminum alloy materials were considered for
206 the matrix in this study. The Table 1 shows the matrix properties used for the simulated air
207 preheaters cases, where c_m and ρ_m are the specific heat and the density of matrix,
208 respectively.

209

210

211

Table 1. Matrix properties of the regenerative air preheater.

| Material | c_m (J/kg K) | ρ_m (kg/m ³) |
|------------------------------|----------------|-------------------------------|
| 2024-T6 aluminum | 875 | 2,770 |
| AISI 1010 alloy carbon steel | 434 | 7,832 |

212

213

214

2.5 Computer Program

215

216

217

218

219

220

221

222

223

224

A computer program written in C programming language was developed for the simulation of regenerative air preheater. The Dev-C++ software was used for compilation and recording results. Three typical sizes of equipment were simulated: small, medium-sized and large. The material AISI 1010 low alloy carbon steel was used for the medium-sized and the large heat exchangers in the simulations. The 2024-T6 aluminum alloy was used for the small air preheater. The total heat transfer in the air preheater, the pressure drop and the outlet temperatures of gas streams were calculated for different porosity levels of the matrix from the prescribed mass flow rate for each gas stream. The other geometrical parameters of the equipment were fixed.

225

226

227

228

229

230

231

232

233

234

235

236

An iterative process was used to obtain the fluid flow and the heat transfer. An outlet temperature values of each stream was assumed at the beginning of this process. Then, the fluid properties were evaluated at the average temperature of each gas stream. Based on these properties, the fluid flow and the heat transfer were obtained from correlations and the Effectiveness-NTU method for regenerative air preheaters. The iterative process continued until convergence of the outlet temperatures for both streams. The whole process was repeated for each assumed matrix porosity value. The subrelaxation factor of 0.5 was used to the convergence of the outlet temperature values. The tolerance for convergence iterative procedure was adjusted as 10^{-3} for the outlet temperatures. The calculations were performed considering the steady-periodic condition of the regenerator, indicating that the temperatures no longer changed in any angular or axial position of the matrix.

237

238

239

240

241

242

243

244

245

246

In order to check the reliability of the developed computer program, the outlet temperatures of gas streams were calculated at a medium-sized rotary regenerator with corrugated ducts. The results were compared with those obtained by Mioralli [34], who numerically simulated the equipment using the finite volume method and compared the numerical results with field data. Table 2 shows the comparison between the results of the present study and those of Mioralli [34]. It is observed that the results are in good agreement.

247
248

Table 2. Comparison of the present data with those of Mioralli [34].

| Outlet Temperature (°C) | Present work | Mioralli [34] | Difference |
|-------------------------|--------------|---------------|------------|
| $T_{c,o}$ | 441.26 | 428.92 | 0.028 |
| $T_{h,o}$ | 160.51 | 142.43 | 0.113 |

249
250
251
252
253
254
255
256
257
258
259

3. RESULTS AND DISCUSSION

The input data of the computer program developed for the simulations are listed in Table 3. The operational conditions of the regenerators are based on information found in the literature and industry. The simulations were carried out from a variation of porosity values in the range of 0.2 to the last value that would guarantee both gas streams of the equipment in laminar regime.

Table 3. Input data for computer program of typical regenerative air preheaters.

| Air Preheater | L (m) | e (m) | D (m) | n (rpm) | Inlet Temp. (°C) | | Flow Rate (kg/s) | |
|---------------|-------|---------|-------|---------|------------------|-----------|------------------|-------------|
| | | | | | $T_{h,i}$ | $T_{c,i}$ | \dot{m}_h | \dot{m}_c |
| Small | 0.2 | 0.00035 | 0.7 | 8 | 50 | 20 | 0.68 | 0.76 |
| Medium-sized | 1.5 | 0.00050 | 6.0 | 3 | 450 | 80 | 39.00 | 62.00 |
| Large | 3.5 | 0.00060 | 15.0 | 2 | 600 | 150 | 292.50 | 411.30 |

260
261
262
263
264
265
266
267
268
269
270
271
272
273
274
275
276
277
278
279
280
281
282

3.1 Thermal Exchange and Pressure Drop Analysis

Graphics with the heat transfer and the pressure drop as function of porosity values are presented for each regenerative air preheater. It is observed that the heat transfer increases and the pressure drop decreases as the porosity values increase for all analyzed cases. In this study is assumed as good thermal exchange a heat transfer value whose reduction is less than 40% when compared with the higher heat transfer value (obtained for $\sigma = 0.2$) in the simulated cases. In addition, it is considered low pressure drop the typical values for the regenerative air preheaters.

Fig. 2 shows the total heat transfer in the small regenerative air preheater and the pressure drop of both gas streams as a function of the matrix porosity. It is observed that from the porosity value around 0.5, the heat transfer in the equipment begins to decrease more significantly. The pressure drop for both gas streams behaves similarly. The typical pressure drop values for the small regenerative air preheater are lower than 200 Pa [35], corresponding to porosity values greater than $\sigma = 0.7$. For the porosities $\sigma = 0.7$ and $\sigma = 0.76$, the percentages of the decrease in the heat transfer are, respectively, 22% and 33% when compared to the highest value $Q \cong 20.5 kW$ for $\sigma = 0.2$. The decrease of heat transfer is around 40% for $\sigma = 0.77$ when compared to the heat transfer obtained for $\sigma = 0.2$. So, the range $0.70 \leq \sigma \leq 0.76$ can be assumed as porosity values that provide a good thermal exchange and low pressure drop for the typical small regenerative air preheater.

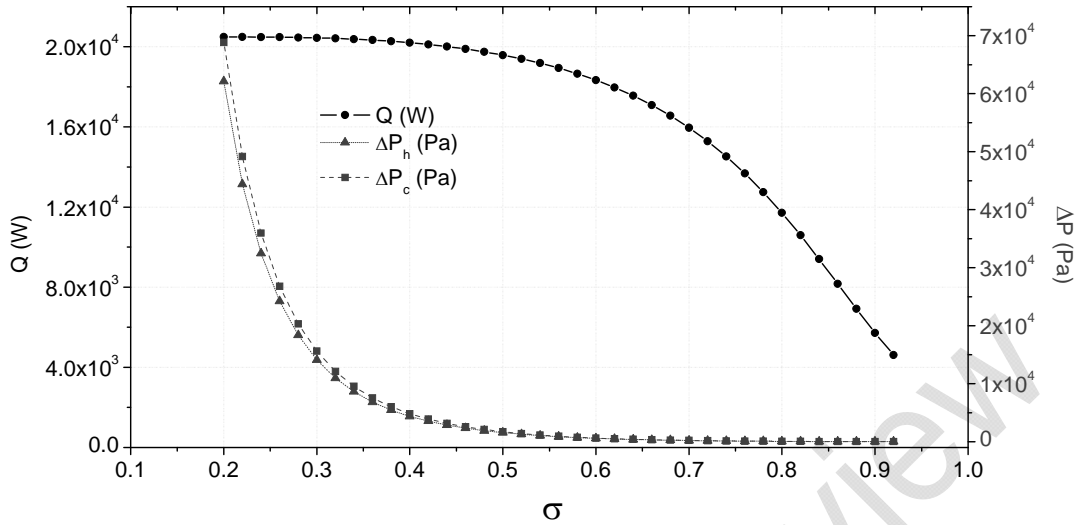
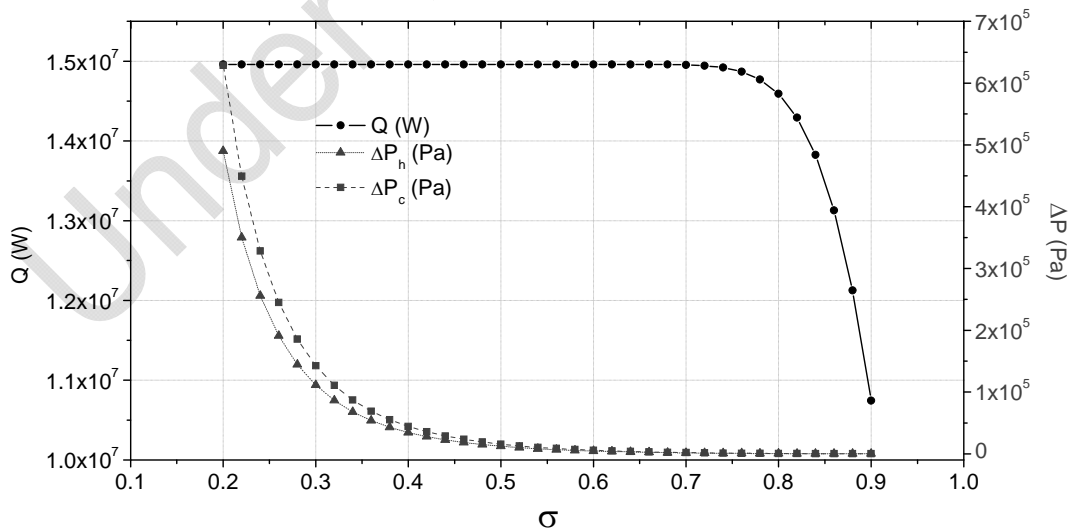


Fig. 2. Heat transfer and pressure drop versus porosity for small regenerative air preheater.

283
284
285
286
287
288
289
290
291
292
293
294
295
296
297
298

Fig. 3 shows the total heat transfer in the medium-sized regenerative air preheater and the pressure drop of both gas streams as a function of the matrix porosity. For this exchanger, the pressure drop values are in the range of up to about 350 Pa for typical operating conditions [35]. Based on this information, the range $0.83 \leq \sigma \leq 0.90$ can be assumed as porosity values that provide a good thermal exchange and low pressure drop for the typical medium-sized regenerative air preheater. This range taking into account the decrease of heat transfer in the equipment less than 40% when compared to the heat transfer ($Q \cong 15 MW$) obtained for $\sigma = 0.2$. The range also includes the pressure drop values lower than 350 Pa. In this simulation, porosity values greater than 0.9 imply a turbulent flow regime for at least one of the gas streams, which is not the object of the present study.

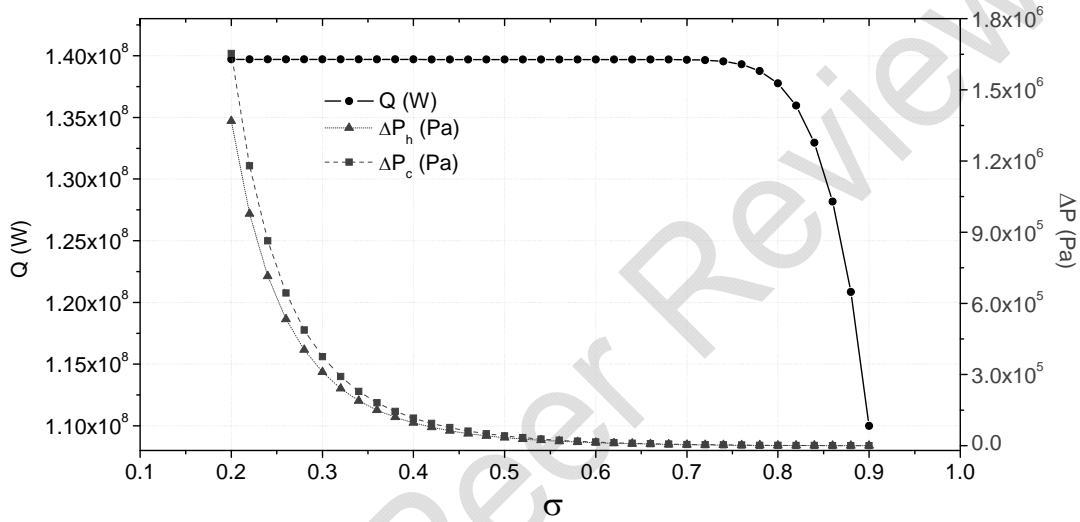


299
300
301
302

Fig. 3. Heat transfer and pressure drop versus porosity for medium-sized regenerative air preheater.

303
 304
 305
 306
 307
 308
 309
 310
 311
 312
 313
 314

Analogously to that observed in Figs. 2 and 3, Fig. 4 shows the total heat transfer in the large regenerative air preheater and the pressure drop of both gas streams as function of the matrix porosity. The pressure drop values observed in the large air preheater for typical operating conditions are in the range of up to about 600 Pa [35]. Considering this aspect and the decrease of heat transfer less than 40% when compared to the heat transfer ($Q \cong 0.14 \text{ GW}$) obtained for $\sigma = 0.2$, the range $0.86 \leq \sigma \leq 0.90$ can be assumed as porosity values that provide a good thermal exchange and low pressure drop for the typical large regenerative air preheater. In this case, porosity values greater than 0.9 imply a turbulent flow regime for at least one of the gas streams, as happened to the simulation of medium-sized regenerative air preheater.



315
 316
 317
 318
 319

Fig. 4. Heat transfer and pressure drop versus porosity for large regenerative air preheater.

320
 321
 322
 323
 324

A simultaneous analysis of Figs. 2, 3 and 4 shows that the assumed ranges of porosity values that provide a good thermal exchange and low pressure drop moves to the right on the abscissa axis as the dimensions and typical operational conditions of the regenerative air preheaters increase. It is also observed that the assumed porosity ranges for the three simulated cases are relatively narrow.

325
 326
 327
 328
 329
 330

A larger porosity range could be established if higher values for pressured drop in the heat exchanger were considered. However, this would imply higher pumping power and energy costs. On the other hand, for the considered pressure drop values, the assumed porosity range could be even smaller if the desired reduction for a good thermal exchange was less than 35% or 30% when compared to the heat transfer obtained for $\sigma = 0.2$.

331
 332
 333

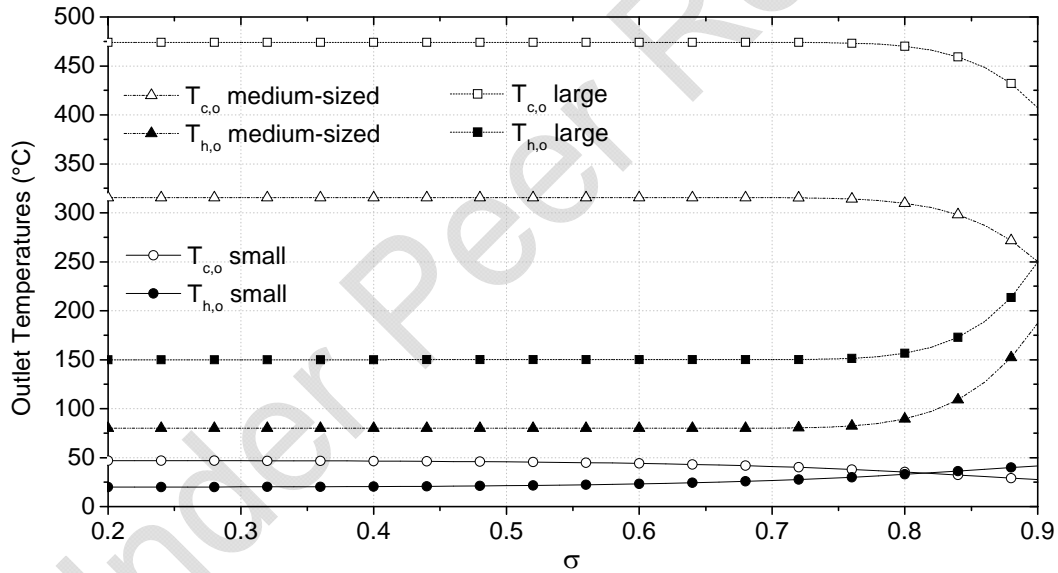
3.2 Outlet Temperatures Analysis

334
 335
 336
 337
 338

The behavior of the outlet temperatures of cold ($T_{c,o}$) and hot ($T_{h,o}$) streams as function of the porosity is show in Fig. 5 for the three typical regenerative air preheaters. It is observed, for all cases, that the outlet temperature values does not change significantly for low porosity values. The outlet temperatures remain practically constant with $\sigma \leq 0.64$ for small heat exchanger and $\sigma \leq 0.75$ for medium-sized and large regenerative air preheaters. This is

339 because small porosity values imply a greater area of thermal exchange and high heat
 340 transfer. The hot stream experience the greatest temperature variation and the outlet
 341 temperature of hot stream is very close to the inlet temperature of cold stream. The mass
 342 flow rate values strongly contributes to this, since the mass flow rate of the hot stream is
 343 smaller than that of the cold stream for all cases. On the other hand, the outlet temperature
 344 of cold stream is less than the inlet temperature of hot stream for the three simulated
 345 preheaters: $T_{c,o} \cong 0.9 T_{h,i}$ for the small exchanger, $T_{c,o} \cong 0.7 T_{h,i}$ for the medium-sized air
 346 preheater and $T_{c,o} \cong 0.8 T_{h,i}$ for the large equipment. Although these outlet temperature
 347 values are significant, the pressure drop is high under these operating conditions. As a
 348 comparison, for porosity values within the range that provides a good thermal exchange and
 349 low pressure drop, $T_{c,o} \cong 0.7 T_{h,i}$ (with $\sigma = 0.74$), $T_{c,o} \cong 0.45 T_{h,i}$ (with $\sigma = 0.86$) and
 350 $T_{c,o} \cong 0.5 T_{h,i}$ (with $\sigma = 0.88$) for the small, medium-sized and large regenerative air
 351 preheaters, respectively.

352
 353 Finally, the results shown in Fig. 5 are consistent with those of Figs. 2, 3 and 4. For the
 354 porosity values in which the total heat transfer starts to decrease in Figs. 2, 3 and 4, the
 355 difference between the values of cold and hot outlet temperature also begins to decrease in
 356 Fig. 5.
 357



358
 359
 360 **Fig. 5. Outlet temperatures versus porosity for small, medium-sized and large**
 361 **regenerative air preheaters.**
 362

363 4. CONCLUSION

364
 365 Three typical regenerative air preheaters were computationally investigated from the pre-
 366 established mass flow rate for each gas stream of the equipment and different matrix
 367 porosity values. Porosity values that provide a good thermal exchange and low pressure
 368 drop were selected for each simulated typical regenerative air preheater. The results showed
 369 that the selected porosity ranges are narrow and moves to the right on the abscissa axis as
 370 the dimensions and typical operational conditions of the heat exchangers increase.

371 Nonetheless, the extent of porosity range may vary according to the desired limits for the
372 heat transfer and the pressure drop of gas streams.

373

374 The outlet temperatures of gas streams were also analyzed as function of porosity. The
375 behavior of the outlet temperatures was consistent with the behavior of the total heat transfer
376 for the three simulated regenerative air preheaters. The obtained results can contribute to
377 the definition of operational conditions of regenerative air preheaters in search of better
378 performance.

379

380 **COMPETING INTERESTS**

381

382 Authors have declared that no competing interests exist.

383

384

385 **REFERENCES**

386

- 387 1. Bae YL. Performance of Rotary Regenerative Heat Exchanger - A Numerical
388 Simulation. Doctoral Thesis, Oregon State University. 1986.
- 389 2. Karlsson H., Holm S. Heat Transfer and Fluid Resistances in Ljungstrom Regenerative-
390 Type Air Preheaters. Transactions of the ASME. 1943;65:61-72.
- 391 3. London AL, Kays WM. The Gas-Turbine Regenerator – the Use of Compact Heat-
392 Transfer Surfaces. Transactions of the ASME. 1950;72:611-621.
- 393 4. Harper DB, Rohsenow WM. Effect of Rotary Regenerator Performance on Gas-Turbine-
394 Plant Performance; Transactions of the ASME; 1953;75:759-765.
- 395 5. Lambertson TJ. Performance Factors of a Periodic-Flow Heat Exchanger. Transactions
396 of the ASME. 1958;80:586-592.
- 397 6. Van Den Bulck E, Mitchell J, Klein SA. Design Theory for Rotary Heat and Mass
398 Exchangers – I: Wavy Analysis of Rotary Heat and Mass Exchangers with Infinite
399 Transfer Coefficients. International Journal of Heat and Mass Transfer. 1985;28:1575-
400 1586.
- 401 7. Ghodsipour N, Sadrameli M. Experimental and Sensitivity Analysis of a Rotary Air
402 Preheater for the Flue Gas Heat Recovery. Applied Thermal Engineering. 2003;23:571-
403 580.
- 404 8. Wu Z, Melnik RVN, Borup F. Model-Based Analysis and Simulation of Regenerative
405 Heat Wheel. Energy and Buildings. 2006;38:502-514.
- 406 9. Nóbrega CEL, Brum NCL. Local and Average Heat Transfer Coefficients for Rotary
407 Heat Exchangers. Proceedings of COBEM. 2007; paper code 1119.
- 408 10. Tanthapanichakoon W, Prawarnpit A. New Simple Mathematical Model of a
409 Honeycomb Rotary Absorption-Type Dehumidifier. Chemical Engineering Journal.
410 2002;86:11-15.
- 411 11. Sphaier LA, Worek WM. Analysis of Heat and Mass Transfer in Porous Sorbents used
412 in Rotary Regenerators. International Journal of Heat and Mass Transfer.
413 2004;47:3415-3430.
- 414 12. Harshe YM, Utikar RP, Ranade VV, Pahwa D. Modeling of Rotary Desiccant Wheels.
415 Chemical Engineering & Technology. 2005;28(12):1473-1479.
- 416 13. Sphaier LA. Unified Formulation for Heat and Mass Transfer in Rotary Regenerators.
417 Proceedings of COBEM. 2007; paper code 1290.
- 418 14. Skiepkó T. Experimental Results Concerning Seal Clearances in Some Rotary Heat
419 Exchangers. Heat Recovery Systems and CHP. 1988;8:577-581.
- 420 15. Skiepkó T. Method of Monitoring and Measuring Seal Clearances in a Rotary Heat
421 Exchanger. Heat Recovery Systems and CHP. 1988;8:469-473.
- 422 16. Shah RK, Skiepkó T. Influence of Leakage Distribution on the Thermal Performance of
423 a Rotary Regenerator. Thermal Engineering. 1999;19:685-705.

- 424 17. Skiepko T. Irreversibilities Associated with a Rotary Regenerator and the Efficiency of a
425 Steam Power Plant. *Heat Recovery Systems and CHP*. 1990;10:187-211.
- 426 18. Jassim RK, Habeebullah BA, Habeebullah AS. Exergy Analysis of Carryover Leakage
427 Irreversibilities of a Power Plant Regenerative Air Heater. *Proceedings Institution of*
428 *Mechanical Engineers. Part A: Journal of Power and Energy*. 2004;218:23-32.
- 429 19. Shang W, Besant RW. Effects of Manufacturing Tolerances on Regenerative
430 Exchanger Number of Transfer Units and Entropy Generation. *Journal of Engineering*
431 *for Gas Turbines and Power*. 2006;128:585-598.
- 432 20. Büyükalaca O., Yilmaz T. Influence of Rotational Speed on Effectiveness of Rotary-
433 Type Heat Exchanger. *International Journal of Heat and Mass Transfer*. 2002;38:441-
434 447.
- 435 21. Kays WM, London AL. *Compact Heat Exchangers*. 3rd. McGraw-Hill: New York, U.S.A,
436 1964.
- 437 22. Worsøe-Schmidt P. Effect of Fresh Air Purging on the Efficiency of Energy Recovery
438 from Exhaust Air in Rotary Regenerators. *Rev. Int. Froid*. 1991;14:233-239.
- 439 23. Sunden B, Karlsson I. Enhancement of Heat Transfer in Rotary Heat Exchangers by
440 Streamwise-Corrugated Flow Channels. *Experimental Thermal and Fluid Science*.
441 1991;4:305-316.
- 442 24. Utriainen E, Sunden B. Numerical Analysis of a Primary Surface Trapezoidal Cross
443 Wavy Duct. *International Journal of Numerical Methods for Heat & Fluid Flow*.
444 2000;10(6):634-648.
- 445 25. Comini G, Nonino C, Savino S. Effect of Space Ratio and Corrugation Angle on
446 Convection Enhancement in Wavy Channels. *International Journal of Numerical*
447 *Methods for Heat & Fluid Flow*. 2003;13(4):500-519.
- 448 26. Zhang L. Laminar Flow and Heat Transfer in Plate-Fin Triangular Ducts in Thermally
449 Developing Entry Region. *International Journal of Heat and Mass Transfer*.
450 2007;50:1637-1640.
- 451 27. Mioralli PC, Ganzarolli MM. Temperature Distribution in a Rotary Heat Exchanger.
452 *Proceedings of COBEM*. 2005;paper code 0356.
- 453 28. Mioralli PC, Ganzarolli MM. Influência da Porosidade no Desempenho de um
454 Regenerador Rotativo. *Anais ENCIT*. 2006;CIT06-0549. Portuguese.
- 455 29. Mioralli PC, Ganzarolli MM. Optimal Porosity of a Rotary Regenerator with Fixed
456 Pressure Drop. *Proceedings of ECOS*. 2007:1307-1314.
- 457 30. Mioralli PC, Ganzarolli MM. Thermal Optimization of a Rotary Regenerator with Fixed
458 Pressure Drop. *Proceedings of ENCIT.*, 2008, paper code 7-5302.
- 459 31. Mioralli PC, Ganzarolli MM. Thermal analysis of a rotary regenerator with fixed pressure
460 drop or fixed pumping power. *Applied Thermal Engineering*. 2013;52:187-197.
- 461 32. White FM. *Viscous Fluid Flow*. McGraw-Hill: New York, U.S.A, 1974.
- 462 33. Wark K. *Thermodynamics*. 4th. McGraw-Hill: New York, U.S.A, 1983. Based in NASA
463 SP-273. U. S. Government Printing Office: Washington, 1971.
- 464 34. Mioralli PC. *Análise Térmica de um Regenerador Rotativo*. Master dissertation.
465 FEM/UNICAMP, Campinas-SP:Brazil, 2005. Portuguese.
- 466 35. Mioralli PC. *Transferência de Calor em um Regenerador Rotativo com Perda de Carga*
467 *Estabelecida nos Dutos da Matriz*. Doctoral thesis. FEM/UNICAMP, Campinas-SP:
468 Brazil, 2009. Portuguese.
- 469